



Title	Decomposition of metal alkylamides, alkyls, and halides at reducible oxide surfaces: mechanism of 'clean-up' during atomic layer deposition of dielectrics onto III-V substrates
Author(s)	Klejna, Sylwia; Elliott, Simon D.
Publication date	2014-02-21
Original citation	KLEJNA, S. & ELLIOTT, S. D. 2014. Decomposition of Metal Alkylamides, Alkyls, and Halides at Reducible Oxide Surfaces: Mechanism of 'Clean-up' During Atomic Layer Deposition of Dielectrics onto III–V Substrates. <i>Chemistry of Materials</i> , 26, 2427-2437. http://dx.doi.org/10.1021/cm403336c
Type of publication	Article (peer-reviewed)
Link to publisher's version	http://dx.doi.org/10.1021/cm403336c Access to the full text of the published version may require a subscription.
Rights	© 2014 American Chemical Society. This document is the Accepted Manuscript version of a Published Work that appeared in final form in <i>Chemistry of Materials</i> , copyright © American Chemical Society after peer review and technical editing by the publisher. To access the final edited and published work see http://dx.doi.org/10.1021/cm403336c
Item downloaded from	http://hdl.handle.net/10468/2421

Downloaded on 2017-02-12T05:56:30Z

- 1
- 2
- 3
- 4
- 5
- 6
- 7
- 8
- 9
- 10
- 11
- 12

- 5
- 6
- 7
- 8
- 9
- 10
- 11
- 12

6
7
8
9
10
11

7
8
9
10
11

8
9
10
11
12

13 **ABSTRACT:** The pairing of high- k dielectric materials with high electron mobility semiconductors for
14 transistors is facilitated when atomic layer deposition (ALD) is used to deposit the dielectric film. An
15 interfacial cleaning mechanism ('clean-up') that results in consumption of semiconductor native oxides
16 and in practically sharp dielectric/semiconductor interfaces has been observed during ALD of Al_2O_3 ,
17 HfO_2 , TiO_2 and Ta_2O_5 with various degrees of success. We undertake a comprehensive study using
18 density functional theory (DFT) to explain differences in the performance of various classes of
19 precursor chemicals in removing native oxide from III-V substrates. The study covers the metals Ta(V),
20 Ti(IV), Zr(IV), Hf(IV), Al(III), Mg(II) combined with methyl, amide and chloride ligands. Of these, we
21 show that clean-up is most effective when depositing MgO. Clean-up with metal alkylamides has a
22 similar mechanism to clean-up with metal methyls insofar as oxygen is scavenged by the metal. The
23 difference in operation of alkylamide and methyl ligands lies in the affinity of the ligand to the
24 substrate. Alkylamide is shown to be prone to decomposition rather than the migration of the entire
25 ligand evinced by methyl. We investigate the multi-step chemical processes associated with
26 decomposition of alkylamide. These processes can also occur during later cycles of high- k ALD and
27 give a chemical vapor deposition (CVD) component to the ALD process. These transformations lead to
28 formation of clean-up products such as aziridine, ethene, N-methyl methyleneimine, hydrogen cyanide
29 and methane. Some – but not all – of the reactions lead to reduction of surface As_2O_3 (*i.e.* clean-up).
30 These results explain the experimentally-observed accumulation of metallic arsenic and arsenic
31 suboxide at the interface. Such understanding can help achieve control of oxide-semiconductor
32 interfaces through the appropriate choice of chemical precursor.

33 **KEYWORDS** atomic layer deposition (ALD), high- k dielectrics, III-V substrate, reducible oxide, clean-
34 up effect, ALD precursor, metal alkylamide, ligand decomposition, density functional theory (DFT)

35

36 1. Introduction

37 The extensive research on pairing of high- k dielectrics materials with high electron mobility
38 semiconductors has renewed interest in replacing SiO₂/Si based transistors for future generations of
39 nanoelectronic devices. The key issue in combining high- k materials for the gate, such as Al₂O₃ and
40 HfO₂, with GaAs or InGaAs III-V semiconductors for the channel is finding a stable passivation of the
41 interface with acceptably low density of interface states. Several reports suggest that this can be partially
42 achieved during deposition of the dielectric film using atomic layer deposition (ALD)¹. The early stages
43 of ALD growth determine the interface properties and therefore careful optimization of deposition
44 conditions helps with improving device performance. An interfacial cleaning mechanism that results in
45 consumption of semiconductor native oxides and in practically sharp dielectric/semiconductor interfaces
46 has been observed during ALD of Al₂O₃², HfO₂³, TiO₂⁴ and Ta₂O₅⁵ on GaAs and InGaAs. This has
47 been called ‘clean-up’ or ‘self-cleaning’. Although removing native oxides is not sufficient to solve the
48 Fermi-level pinning problem in devices⁶, it is an important step in the preparation of abrupt interfaces.
49 The electrical characteristic of the device is improved though when appropriate and optimised
50 passivation and ALD processing is enabled as suggested in⁷.

51 While the phenomenon of native oxide thinning during semiconductor exposure to ALD metal
52 precursors has been confirmed in several experiments, the chemistry of this process is not well
53 understood. First reports on the clean-up effect documented an effective passivation of GaAs-based
54 substrates with trimethylaluminium (TMA or AlMe₃; where Me = CH₃) when depositing Al₂O₃⁸. For
55 HfO₂ ALD, the clean-up effect was observed mainly when using hafnium alkylamides, with similar
56 behaviour shown by tetrakis(ethylmethyldamido)hafnium (TEMAH or Hf(NEtMe)₄; where Et = C₂H₅) or
57 tetrakis(dimethylamido)hafnium (TDMAH, Hf(NMe₂)₄)^{3a, 8-9}. A recent study shows that ALD processes
58 utilizing alkylamide precursors featuring Ti (tetrakis(dimethylamido)titanium, TDMAT, Ti(NMe₂)₄) or
59 Ta (pentakis(dimethylamido)tantalum, PDMAT, Ta(NMe₂)₅) also result in the same interfacial cleaning
60 effect while depositing TiO₂ or Ta₂O₅ respectively^{4b, 5}. These observations indicate that the common

61 requirement for self-cleaning is the use of organometallic or metalorganic precursors. However, the
62 examples of the purely inorganic HfCl_4 and TiCl_4 ALD processes contradict this assumption. ‘Clean-up’
63 is also observed with the use of these precursors by Delabie *et al.* ^{3b} and Granados-Alpizar and Muscat
64 ^{4a} but was not reported by Frank *et al.* ¹⁰.

65 Common experimental observations are found for interfacial cleaning with TMA and alkylamide
66 precursors. Generally arsenic oxides are easier to remove than gallium oxides. Higher oxidation states of
67 both As (As^{5+}) and Ga (Ga^{3+}) are more sensitive to reduction. Accumulation of metallic arsenic –
68 arsenic suboxide at the interface has been observed for TMA based ALD ^{6a} and alkylamide based ALD
69 ⁹. It seems that elevating the temperature of the process significantly enhances the clean-up abilities of
70 alkylamides, and this differentiates these processes from TMA-based clean-up ^{5, 11}. Granados-Alpizar
71 and Muscat show differences in surface reactions during GaAs exposure to TMA and TiCl_4 pulses ^{4a}.
72 both precursors remove the native oxide layer, but the mechanisms underlying this process seem to be
73 fundamentally different. TMA deposits an Al_2O_3 layer and removes a portion of As from the surface,
74 whereas TiCl_4 removes O and leaves the surface passivated with Cl atoms. The mechanism for
75 removing oxides with the use of HfCl_4 differs also from the one for TiCl_4 . The growth of hafnium oxide
76 is enhanced ^{3b} and growth of titanium oxide is inhibited ^{4a}. These extensive and sometimes conflicting
77 studies on interfacial self-cleaning show how little is understood about the chemistry occurring in the
78 initial cycles of deposition of dielectrics.

79 In this study with the use of DFT we try to provide improved understanding of the chemical principles
80 underlying ‘clean-up’ and thus rationalize experimental observations. There are not many studies
81 available on mechanisms during early stages of growth on III-V semiconductors. Typical mechanisms
82 occurring during ALD on other semiconductors (Si, Ge) are described in numerous publications, as
83 reviewed by Elliott ¹². Previous atomic-scale simulations of clean-up mechanisms focused on the
84 interaction of TMA with GaAs ¹³ and III-V native oxides ¹⁴. TMA was shown to be able to reduce
85 arsenic oxides into gaseous As_4 and solid GaAs, with Al_2O_3 formation and C lost as C_2H_6 ¹⁴. DFT

86 revealed that the mechanistic step of reduction takes place when the CH_3 ligand migrates from surface-
87 bound Al/As/Ga to O and gets oxidised, simultaneously reducing the III-V native oxide substrate. From
88 the TMA example two interesting conclusions emerge: ligand exchange as well as ligand redox
89 mechanisms are at play during clean-up and the precursor metal cation provides an energetic sink when
90 it bonds to oxygen.

91 In the current investigation, building on the example of TMA, we look for an explanation of differences
92 observed in the operation of different families of metal precursors: alkylamides, methyls and chlorides.
93 We focus mainly on the clean-up of the arsenic (III) oxide component of the surface utilizing the
94 $\text{Hf}[\text{N}(\text{CH}_3)_2]_4$ precursor during HfO_2 ALD. The choice of the surface model has been previously
95 motivated and its structure and limitations have been described in detail ¹⁴. The main emphasis here is
96 on the interaction of the dimethylamido ligand (dma) with the oxide surface with a view to finding
97 potential redox properties of this ligand. Based on the TMA findings, the metal cation is assumed to be
98 redox inactive, and to combine with oxide anions to form a dielectric oxide. We postulate that formation
99 of the dielectric oxide is the driving force for the clean-up effect and confront this by investigating the
100 clean-up ability of precursors that are chemically different to TMA. Assuming these postulates allows
101 us to define and separate the factors governing the clean-up effect. In this way, a set of general reactions
102 is generated and a comparison can be made between a number of different precursors. In the end, this
103 approach should help with assessing whether clean-up is a general effect, regardless of precursor being
104 used.

105 **2. Computational method & approach**

106 Periodic density functional theory (DFT) at 0 K as implemented in the VASP package ¹⁵ was applied as
107 a reliable method for computation of the ground state electronic structure and total energy of crystalline
108 materials. We use the generalized gradient approximation (GGA) of Perdew and Wang (PW91) ¹⁶ for
109 the exchange-correlation energy. The core electrons were described with ultrasoft pseudopotentials

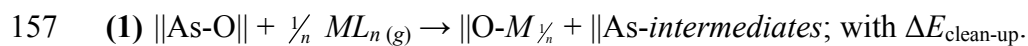
110 (USPP) ¹⁷ projected into real space and valence electrons were described with a plane-wave basis with a
111 kinetic energy cutoff of 396 eV. Geometry optimization was carried out with a sparse Monkhorst-Pack
112 k -point sampling of reciprocal space. A conjugate-gradient algorithm was used for ionic relaxation with
113 all ions relaxed until the forces on the ions were less than 0.02 eV/Å.

114 High accuracy was used for bulk oxide calculations: convergence of energies to 10^{-4} eV with respect
115 to coordinates of ions and cells, 130% of the standard plane-wave cutoff energy, convergence with
116 respect to k -point sampling. The total energy versus volume for all models of the bulk oxide structures
117 was optimized resulting in equilibrium lattice parameters that agreed well with experiment (with
118 deviation less than 2%) ¹⁸. Lattice parameters and space groups, along with k -point sampling for these
119 calculations are given in the supporting information. We used experimental lattice constants for the bulk
120 model of *arsenolite* arsenic (III) oxide ¹⁹ since its crystalline structure did not allow us to perform cell
121 shape optimization within DFT as explained in detail before ¹⁴. Ions were fully relaxed within the fixed
122 As₂O₃ cell and the structural parameters compared well with the experimental values. The *arsenolite*-
123 As₂O₃ (010) surface is modeled by periodic slabs separated by 10 Å of vacuum. We use a 2×2 surface
124 expansion that contains 1 layer totaling 8 molecular units of As₄O₆ (80 atoms) and a 2×2×1 k -point
125 mesh for surface calculations. This surface is computed to have a surface energy below 0.02 J/m².
126 Gaseous species (precursor molecules and gas phase products) were individually relaxed in a simulation
127 box, cubic or rhombohedral, of dimensions 15×15×15 Å, with six k -points located at the edges of the
128 first Brillouin zone. Geometrical parameters for all optimised gaseous molecules can be found in the
129 supporting information.

130 For investigation of the ligand decomposition surface reactions we use the bare As₂O₃ (010) surface. For
131 redox reactions differences in Bader atomic charges ²⁰, Δq , are analyzed to determine the chemical state
132 of intermediates and thus help in predicting a final product. The sign convention used in this paper is
133 that $\Delta q < 0$ means loss (oxidation of an atom) and $\Delta q > 0$ means gain (reduction of an atom) of electron
134 population on atoms taking part in the considered reaction. To study the stability of surface bound

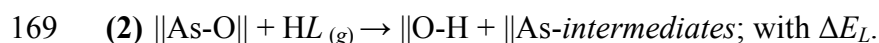
intermediates we performed DFT molecular dynamics in the canonical ensemble at around 300° C for 0.4 ps. At the end of these simulations all surface intermediates were found to be bonded the same as their initial configuration, suggesting that no spontaneous reactions occur and that there are barriers to overcome on the potential energy surface for any following chemical transformations. We neglect the constant contribution to entropy (S) from solid surfaces with adsorbates since S^{trans} and S^{rot} for surfaces are approximately zero and S^{vib} is approximately constant during the reaction, $\Delta S^{\text{vib}} = 0$. Therefore $\Delta S = 0$ for surface reactions and the Gibbs free energy profiles closely resemble the DFT potential energy surfaces. Reaction energetics are computed with an estimated accuracy of 0.1 eV. Activation energies reported here were computed using the nudged elastic band method (NEB)²¹. We used up to 8 images for each reaction pathway. The damped molecular dynamics algorithm for ionic relaxation was found to be appropriate for the regarded system. Around 1000 steps were needed to converge forces on atoms to below 0.05 eV/Å.

In this investigation we consider the process where the adsorbed metal precursor molecules, with the general formula ML_n ($M = \text{Mg(II)}, \text{Al(III)}, \text{Ti(IV)}, \text{Zr(IV)}, \text{Hf(IV)}, \text{Ta(V)}$; $L = [\text{N(Me)}_2]^-, [\text{Me}]^-, [\text{Cl}]^-$; n – oxidation state of metal), undergo a series of clean-up transformations leading to removal of the native oxides of III-V substrates. As outlined in section 1, we propose that the main and most thermodynamically stable product of these transformations is a film of dielectric metal oxide with the general formula M_2O_n . (Thus, there is no reduction or oxidation of M). Another factor in the successful clean-up performance is affinity of the precursor ligand L to the III-V oxide substrate. We can describe formation of one O- M bond and subsequent transformations of the ligand on the sample III-V oxide surface (*i.e.* a clean-up process) with the following equation where \parallel stands for surface bound species and g for gas-phase molecules:

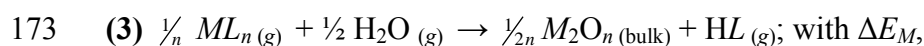


In the above equation we assume that the formed metal oxide is stoichiometric: upon increasing the coordination number of the metal centre to the native oxide oxygen, the coordination to the ligands

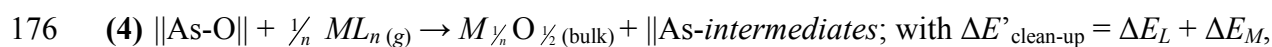
decreases and ligands are released to interact with the substrate. The equation also shows that M -O formation and interaction of ligands with As can be viewed as separate events, to a first approximation. Identification of these separate factors allows for an efficient description of interactions of the surface *intermediates* that are formed as a result of ligand decomposition, and of associated chemical processes that lead to formation of the clean-up products. Computing the *intermediates* from just one ligand should be computationally less expensive and easier to understand than computing the decomposition of the entire precursor molecule. Therefore, in this paper we take advantage of this methodology and reduce equation (1) to a description of chemical processes associated only with the interaction of one ligand with the substrate independent of M , as per the reaction:



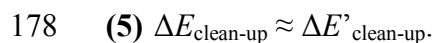
A proton is included to ensure overall charge neutrality and so on the right hand side of the reaction a hydroxyl group $\|O-H$ is formed. The formation of one M -O bond in equation (1) can then be described by the model reaction for various M :



which is the overall ALD reaction. Combination of the ligand reaction (2) and the metal-dependent correction (3) gives essentially reaction (1):



but at much lower computational effort. Therefore:



Because of limitations of our current model, we cannot generally compute the complete energetics for each mechanism here. As we focus in this study on the decomposition of the dma ligand and its redox properties, our model naturally does not cover molecular or dissociative adsorption of the precursor and associated steric effects. Nevertheless, for validation purposes we performed explicit simulation of the dissociative adsorption of the whole precursor molecule according to equation (1). In Table 1 we compare energetics obtained for adsorption and ligand dissociation for three different precursors:

185 Hf(NMe₂)₄, AlMe₃, TiCl₄. The ‘whole precursor’ approach gives a $\Delta E_{\text{clean-up}}$ that agrees well with the
 186 $\Delta E'_{\text{clean-up}}$ value from the ‘ligand only’ approach in all three cases, thereby strongly supporting the latter
 187 approach. Additionally the ‘whole precursor’ approach for the Hf(NMe₂)₄ precursor was used for the
 188 NEB calculation of activation energies, which is reported in the Results and Discussion section.

189

190 Table 1. Validation of the investigated model: energies $\Delta E_{\text{clean-up}}$ for reaction of precursor adsorption
 191 and dissociation of the ligand from the metal center according to reaction $\parallel\text{As-O}\parallel + \frac{1}{n} ML_n(g) \rightarrow \parallel\text{O-}$
 192 $M \frac{1}{n} + \parallel\text{As-L}$ compared to $\Delta E'_{\text{clean-up}}$ obtained from the model ‘ligand only’ reaction $\parallel\text{As-O}\parallel + \frac{1}{n} ML_n(g)$
 193 $\rightarrow M \frac{1}{n} O \frac{1}{2}(\text{bulk}) + \parallel\text{As-L}$. Surface models showing product of this reaction on the example of Hf[N(Me₂)₄
 194 precursor are available in the supporting information. Simulations were performed using identical
 195 computational parameters for both approaches.

Metal precursor	$\Delta E_{\text{clean-up}}$ [eV]	$\Delta E'_{\text{clean-up}}$ [eV]
Hf(NMe ₂) ₄	-1.0	-1.0
AlMe ₃	-1.2	-1.3
TiCl ₄	-0.2	-0.2

196

197 In section 3.1 thermodynamic energies are presented for formation of metal oxides from gas phase
 198 precursors determined using DFT, ΔE_M (equation (3)). In the subsequent sections different types of
 199 *intermediates* that are formed during clean-up as a result of decomposition of selected precursors are
 200 examined and their structures are illustrated in Figure 2. Types of reactions included are: dissociation of
 201 the precursor through scission of the *M-L* bond in section 3.2, decomposition of the dma ligand through
 202 scission of the C-H and N-C bonds in section 3.3 and multiple decomposition steps combining these
 203 elementary steps described in section 3.4. Energetics for the interaction of ligands with the substrate,
 204 ΔE_L , is given in Table 2. The effectiveness of different metal precursors in performing clean-up of III-V
 205 oxides is evaluated by correcting ΔE_L with ΔE_M (also Table 2). ΔE_M and ΔE_L along with overall $\Delta E'_{\text{clean-}}$

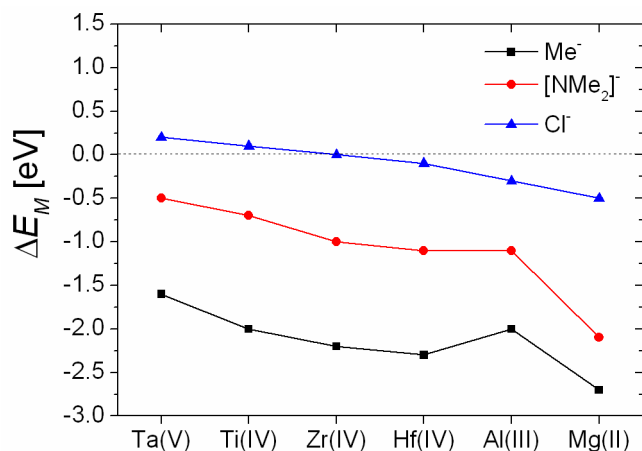
up are summarized in Figure 1 and Figure 3. A reaction scheme considered for the decomposition of the dma ligand is illustrated in Figure 4. A series of proposed elementary steps can give rise to desorption of multiple clean-up products. Based on the thermodynamic accessibility of these elementary surface steps and some kinetic indications, we discuss in each section which clean-up mechanism and associated by-product is competitive in the ALD process.

3. Results and Discussion

3.1. Formation of metal oxides from gas phase precursors

Reaction (3) contains information about the reactivity of precursors towards formation of bulk oxide and bonding changes upon elimination of ligands as HL. Computed energetics for a selection of metals and ligands are summarized and illustrated in Figure 1. Values for reaction (3) can be found in Table 2 under $\Delta E'_{\text{clean-up}}$ for $\Delta E_L = 0$ eV (see equations (3) and (4)).

Figure 1. Computed energetics, ΔE_M , for formation of metal oxides from gas phase precursors ML_n (x axis: $M = \text{Mg(II)}$, Al(III) , Ti(IV) , Zr(IV) , Hf(IV) , Ta(V) ; $L = [\text{N}(\text{Me})_2]^-$, $[\text{Me}]^-$, $[\text{Cl}]^-$; n = oxidation state of metal) and water according to: $\frac{1}{n} ML_n (\text{g}) + \frac{1}{2} \text{H}_2\text{O} (\text{g}) \rightarrow \frac{1}{2n} M_2\text{O}_n (\text{bulk}) + \text{HL} (\text{g})$ (equation (3)). Lines are to guide the eye.



224 The energetics indicate that the most reactive precursor family for formation of metal oxides and
225 elimination of HL are metal methyls. The most reactive of the six considered is MgMe_2 with $\Delta E_M = -2.7$
226 eV per methyl ligand. The least reactive among the hypothetical methyl precursors is TaMe_5 with ΔE_M
227 $= -1.6$ eV per Me for formation of Ta_2O_5 . AlMe_3 with $\Delta E_M = -2.0$ eV per Me presents similar reactivity
228 to TiMe_4 , not to HfMe_4 or ZrMe_4 . Al, Hf and Zr alkylamides with $\Delta E_M \approx -1.0$ eV per ligand have
229 similar reactivity and the Ta and Ti alkylamides are slightly less reactive. The most reactive for
230 formation of oxide among metal alkylamides is $\text{Mg}[\text{N}(\text{CH}_3)_2]_2$ with $\Delta E_M = -2.1$ eV per alkylamide
231 ligand. According to our computations the smallest driving force for formation of $M_2\text{O}_n$ is shown by
232 chloride precursors. ΔE_M for $L = \text{Cl}^-$ ranges from -0.5 eV per Cl for Mg to $+0.2$ eV per Cl for Ta. In
233 general, the calculations reveal the following order of M reactivity, insensitive to the identity of L :
234 $\text{Mg(II)} > \text{Hf(IV)} \approx \text{Zr(IV)} > \text{Ti(IV)} > \text{Ta(V)}$. The exception is Al(III) which is predicted to change its
235 relative reactivity depending on the nature of L . Relative to the other metals, the Al cation is the most
236 reactive when bonded to chloride ligands and the least reactive, with similar reactivity to Ti(IV), for $L =$
237 Me^- . These trends are consistent with previous calculations²².

249 Table 2. List of possible clean-up *intermediates*: **A-K**, **A'** and **A''** that are formed during ALD III-V
250 substrate exposure to various metal precursors. Energies are in eV relative to $\|As - O\| + HL_{(g)}$ as per
251 reaction (2) with $L = [N(Me)_2]^-$, Me^- , Cl^- . The effect of different $M = Ta, Ti, Zr, Hf, Al, Mg$ is included
252 by adding the correction ΔE_M obtained from reaction (3) (see section 2 for details).

L	products at surface:	ΔE_L	$\Delta E'_{\text{clean-up}}$ for M :					
			Ta	Ti	Zr	Hf	Al	Mg
$[N(Me)_2]^-$	$\ As - O\ + HNMe_{2(g)}$	0.0	-0.5	-0.7	-1.0	-1.1	-1.1	-2.1
	A $\ O - H + \ As - NMe_2$	+0.1	-0.4	-0.6	-0.9	-1.0	-1.0	-2.0
	B $2\ O - H + \ As - N(Me)CH_2 - As\ $	+0.6	+0.1	-0.1	-0.4	-0.5	-0.5	-1.5
	C $2\ O - H + \ As - N(Me)CH_2 - O\ + 2e^-$	+1.3	+0.8	+0.6	+0.3	+0.2	+0.2	-0.8
	D $\ O - H + \ As - N(Me)CH_2 - As\ + \ As - H - 2e^-$	+2.1	+1.6	+1.4	+1.1	+1.0	+1.0	0.0
	E $\ O - H + \ As - N(Me)CH_2 - O\ + \ As - H$	+1.2	+0.7	+0.5	+0.2	0.1	0.1	-0.9
	F $\ O - H + \ As = NMe + \ O - Me$	+1.5	+1.0	+0.8	+0.5	+0.4	+0.4	-0.6
	G $\ O - H + \ As = NMe + \ As - Me - 2e^-$	+1.6	+1.1	+0.9	+0.6	+0.5	+0.5	-0.5
	H $3\ O - H + \ As - N(CH_2 - As\)_2$	+1.3	+0.8	+0.6	+0.3	+0.2	+0.2	-0.8
	I $4\ O - H + \ As = NCH=CH_2 + 2e^-$	+2.2	+1.7	+1.5	+1.2	+1.1	+1.1	+0.1
	J $2\ O - H + \ As - N=CH_2 + \ As - Me$	+0.9	+0.4	+0.2	-0.1	-0.2	-0.2	-1.2
	K $3\ O - H + \ As - N=CH - As\ + \ As - Me$	+1.9	+1.4	+1.2	+0.9	+0.8	+0.8	-0.2
$[Me]^-$	$\ As - O\ + CH_{4(g)}$	0.0	-1.6	-2.0	-2.2	-2.3	-2.0	-2.7
	A' $\ O - H + \ As - Me$	+0.7	-0.9	-1.3	-1.5	-1.6	-1.3	-2.0
$[Cl]^-$	$\ As - O\ + HCl_{(g)}$	0.0	+0.2	+0.1	0.0	-0.1	-0.3	-0.5
	A'' $\ O - H + \ As - Cl$	-0.3	-0.1	-0.2	-0.3	-0.4	-0.6	-0.9

253

254 3.2. Dissociation of ligand by M-L scission

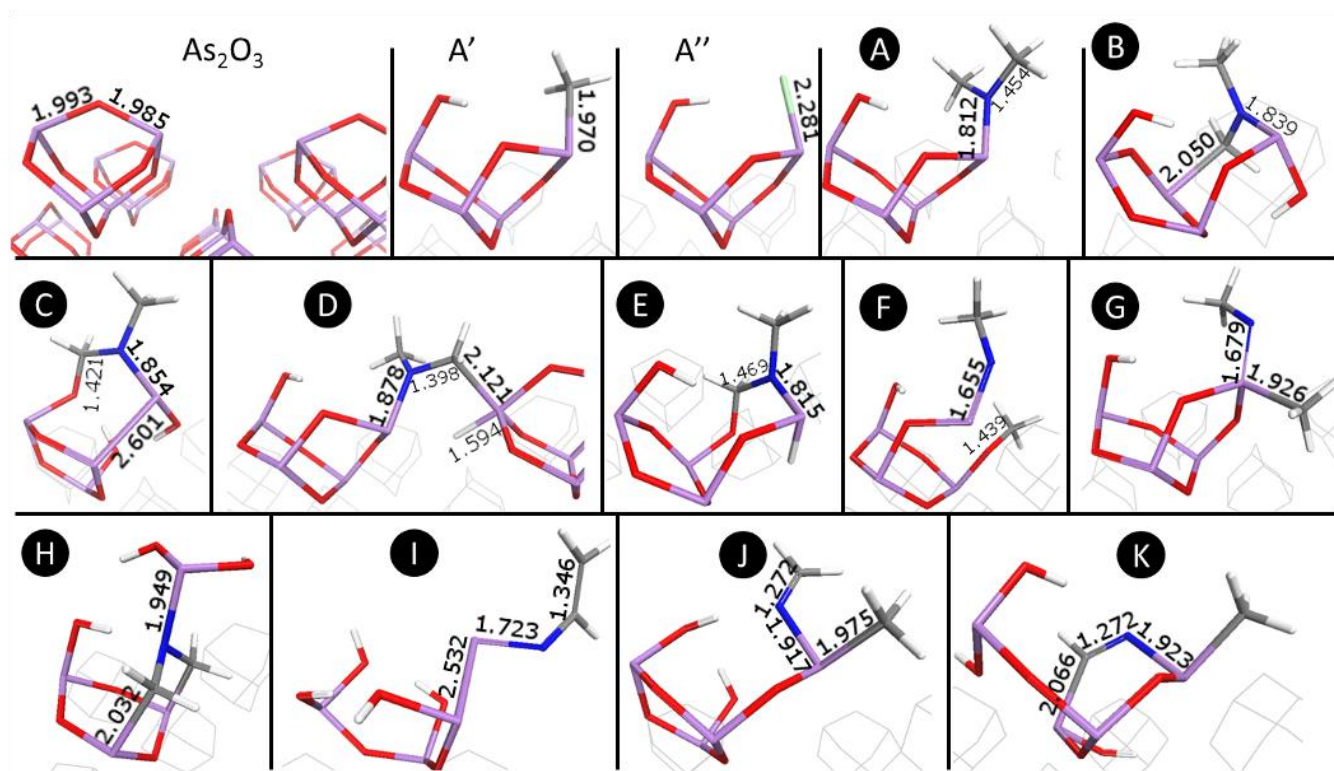
255 By calculating DFT energies for dissociation of the ligand from the metal center, we investigate the
256 affinity of the ligand to the oxide to be cleaned-up. This gives us $\Delta E'_{\text{clean-up}}$ for the elementary step that
257 leads to a ligand exchange mechanism. The elementary steps that we have considered involve the
258 transfer of a dimethylamide, methyl and chloride group to the surface As atom in structures **A**, **A'** and

259 A'' respectively, shown in Figure 2. Energetics for formation of intermediate A show that the
 260 alkylamide ligand can readily dissociate from the M center to the available As site and form a
 261 thermodynamically stable product ||As – N(CH₃)₂ plus oxide of M (see Table 2 and Figure 3 for
 262 energetics). According to reaction (2) and correction for the M-O bond formation, reaction (3), this
 263 ligand transfer process is exothermic for all considered metals. The energy for this reaction ranges from
 264 -0.4 eV per ligand for Ta[N(CH₃)₂]₅ to -2.0 eV for Mg[N(CH₃)₂]₂. This reaction is very facile with a
 265 computed activation energy of just +0.1 eV, and so it will proceed until the surface is saturated with ||As
 266 – N(CH₃)₂ species (the reaction profile for the corresponding reaction of the whole precursor is
 267 available in the supporting information).

268

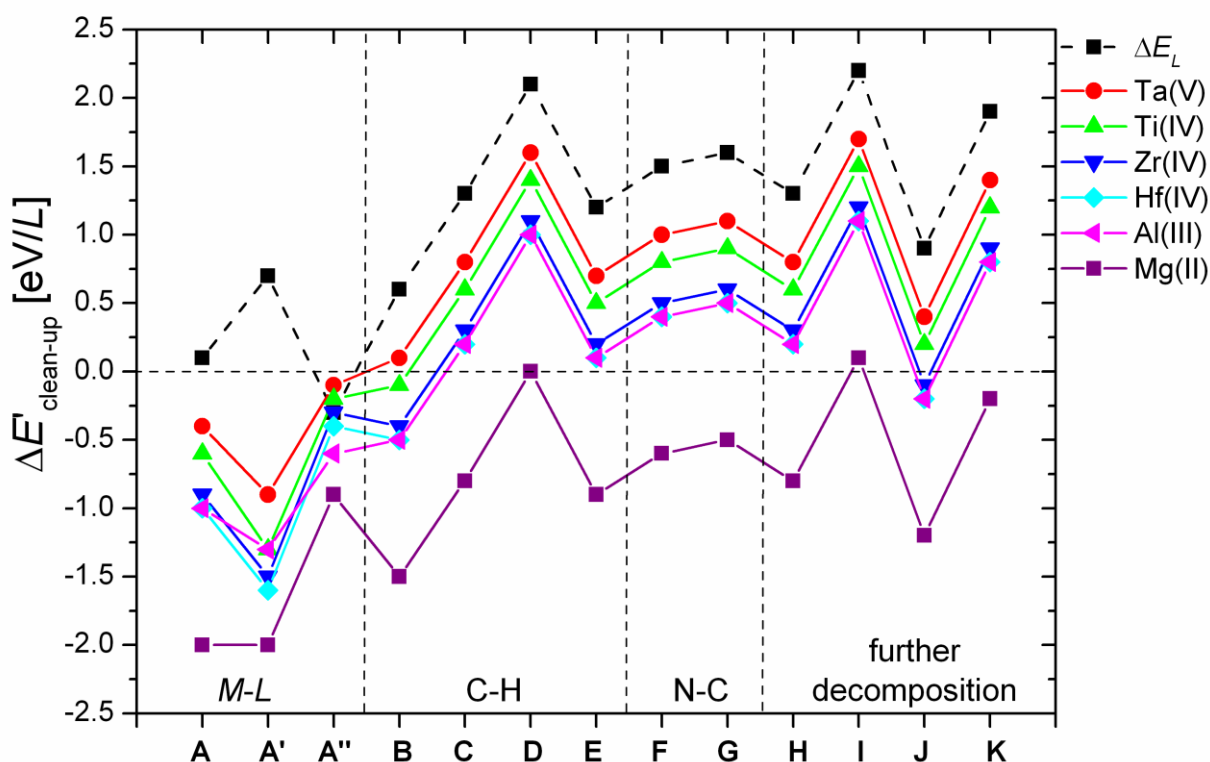
269 Figure 2. Surface models for As₂O₃ and decomposition species of metal methyls, A', metal chlorides,
 270 A'', and metal alkylamides, A-K. Stick representation: purple As, red O, white H, gray C, green Cl,
 271 blue N. Selected bond lengths are given in Å. Thin lines show adjacent substrate atoms.

272



273

Figure 3. Computed energetics for surface intermediates, **A-K**, which are formed during clean-up of As_2O_3 . As listed in Table 2, **A**, **A'** and **A''** are surface products of precursor decomposition through scission of $M-L$ bond ($M = \text{Mg(II)}$, Al(III) , Ti(IV) , Zr(IV) , Hf(IV) , Ta(V)) for $L = [\text{N}(\text{Me})_2]^-$, $[\text{Me}]^-$, $[\text{Cl}]^-$ respectively; **B-E** are surface products of decomposition of $[\text{N}(\text{Me})_2]^-$ through scission of C-H bond; **F** and **G** surface products of decomposition of $[\text{N}(\text{Me})_2]^-$ through scission of N-C bond; **H-K** are surface products when further decomposition occurs through scission of both C-H and N-C bonds. ΔE_L (equation (2)) describes interaction of the ligand L with the As_2O_3 substrate (black datapoints). It is subsequently corrected with ΔE_M (equation (3)) and gives overall $\Delta E'_{\text{clean-up}}$ for various M (equation (4)). Lines are to guide the eye and do not imply a reaction sequence (see instead Figure 4).



Energetics show that the methyl ligand is very reactive towards the arsenic oxide substrate and more reactive than alkylamide (**A'** Figure 3). The energy ranges from -0.9 eV for $\text{Ta}(\text{CH}_3)_5$ to -2.0 eV for $\text{Mg}(\text{CH}_3)_2$. The energy for exchange of a Cl^- ligand between the precursor metal center and the native

oxide, with product A'' in Figure 2, ranges from -0.1 eV for TaCl₅ to -0.9 eV for MgCl₂, indicating that it is less thermodynamically favored than for alkylamides and methyls.

Sufficient concentration of these As – L groups may lead to formation of AsL₃: tris(dimethylamino)arsine, TDMAAs, As[N(CH₃)₂]₃; trimethylarsine, As(CH₃)₃ and arsenic trichloride AsCl₃, as volatile products in processes utilizing alkylamides, methyl and chloride precursors respectively. Desorption of these molecules means that As₂O₃ has been transformed into M₂O_n, *i.e.* clean-up. Indeed, this ligand transfer mechanism has been proposed by others ^{3a, 8} to explain the clean-up effect. Experimental study clearly shows enhancement of the clean-up process with increasing temperature when metal alkylamides are used ^{5, 23}. Even though the first step of the ligand exchange reaction is extremely facile, both thermodynamically and kinetically, significant kinetic requirements may originate from steric effects in subsequent steps. There was evidence for this in our previous study for TMA, where we showed that the rate limiting step for the ligand transfer process could be crowding of methyl ligands at one surface site ²⁴. We suspect that this process can be even more difficult for the bulkier alkylamides. Thus, steric effects may have a pronounced influence on the kinetics of ligand transfer to TDMAAs, which may stop this reaction before going to completion, and promote ligand decomposition instead. In fact, TDMAAs is known to thermally decompose on the GaAs surface ²⁵. Therefore, it is reasonable to suspect that the alkylamide can decompose, or partially decompose, in contact with the native oxide surface, and give rise to other clean-up products rather than form TDMAAs. Ligand decomposition is investigated in subsequent sections.

In the case of chlorides, although they are successfully used in ALD of different metal oxides, there is no agreement in the literature about their interfacial self-cleaning abilities ^{3b, 4a, 10}. One reason may be the lower driving force towards formation of the metal oxide dielectric; Figure 1 shows that formation of the metal oxide during clean-up is an important factor in case of alkylamides and methyls, but a minor factor in the case of chlorides (ΔE_M ranges +0.2 to -0.5 eV). Therefore, we suggest that chloride chemistry is different. Most of the metal chlorides are weak Lewis acids. Their electrophilic

312 characteristic allows them to form Lewis adducts like TaOCl_3 , complexes like $[\text{TiCl}_6]^{2-}$ or even
313 hydrates, *e.g.* $\text{MgCl}_2(\text{H}_2\text{O})_x$ ²⁶. Formation of oxychlorides, *e.g.* TiOCl_2 , or even hydroxychlorides,
314 TiCl_3OH , during clean-up with TiCl_4 for TiO_2 deposition, could explain observed removal of O and
315 surface passivation with Cl ^{4a}. As proposed before, clean-up with this ligand can be accounted for via an
316 agglomeration reaction mechanism ^{3b}.

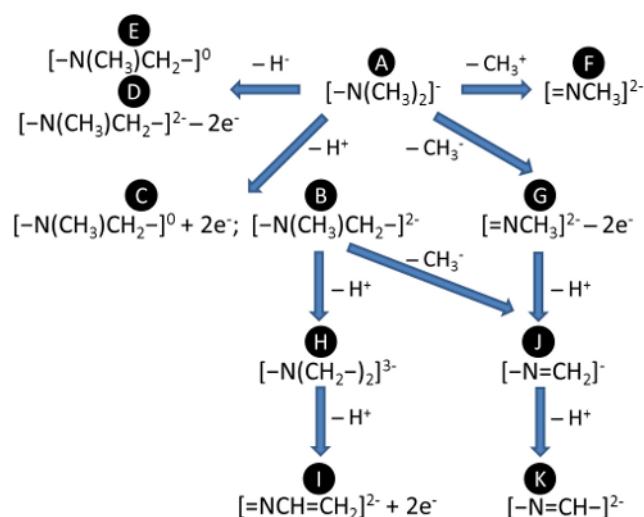
317 Ligand affinity for Ga and In is discussed in section 3.5 .

318 *3.3. Decomposition of dma ligand*

319 For the following consideration of decomposition processes of alkylamide ligand on the example of
320 dimethylamide we use the highly stable product $\text{A} \parallel \text{As} - \text{N}(\text{CH}_3)_2$, as a starting species for further clean-
321 up transformations **B-K**. Decomposition of the alkylamide ligand is possible via activation of a C-H
322 bond, releasing anionic or cationic H, or of an N-C bond, releasing anionic or cationic CH_3 as
323 schematically shown in Figure 4. In this section we examine mechanistic paths for these H and CH_3
324 moieties to attack As and O sites. We consider all possible reactions and highlight redox processes that
325 may enhance the clean-up effect.

326
327
328
329
330
331
332
333
334
335
336
337

Figure 4. Reaction scheme for decomposition of dimethylamido ligand $[-N(CH_3)_2]^-$ on metal oxide surfaces (species **A-K**). Notation: ‘ $-H^{+/-}$ ’ means dissociation of proton/hydride from ligand to the surface; ‘ $-Me^{+/-}$ ’ means dissociation of methylum/methanide group from ligand to the surface; ‘ $+2e^-$ ’ means oxidation of ligand by surface (reduction of surface by ligand); ‘ $-2e^-$ ’ means reduction of ligand by surface (oxidation of surface by ligand).



3.3.1. C-H scission and H elimination (B-E)

The C-H bond of the ligand is weakened by the electron density of the lone pair of electrons on the neighboring N atom, so that H α to the N atom can dissociate and bond to an available surface site. First we investigate scission of the C-H bond and formation of an O-H bond in the intermediate **B** shown in Figure 2. Our calculations show that upon the proton (H^+) transfer from a ligand to a surface O atom, the As-O bond is broken. The electronic density around the C atom in the remaining methylene (CH_2) moiety of the ligand increases by $\Delta q = +1.5e$. This Lewis basic C atom can interact with the surface As cation that lost coordination to the O atom. The bond formed between the As atom and the C atom is 2.0 Å long which is typical of single As-C bond. As a result a N-methylmethylenimido ion ($[-N(Me)CH_2-]^{2-}$) is attached to the surface. Our attempts to find a competitive minimum for the N-methylmethylenimido ligand with tricoordinated N atom featuring a N=C double bond (*i.e.* $[-N(Me)=CH_2]^-$) were not successful. The thermodynamically stable state preserves tricoordinated N and tetrahedral C. This process is the most exothermic of the decomposition processes with a calculated

357 $\Delta E'_{\text{clean-up}}$ ranging from +0.1 eV for Ta[N(CH₃)₂]₅ to -1.5 eV for Mg[N(CH₃)₂]₂ (Table 2, **B**). An
358 activation energy of around +1.4 eV is computed for the example of Hf[N(CH₃)₂]₄ where $\Delta E'_{\text{clean-up}}$ = -
359 0.5 eV (the reaction profile for the corresponding reaction of the whole precursor is available in the
360 supporting information).

361 We also examine the redox process mediated by ligand attack of the CH₂ moiety onto the O site, instead
362 of the As site, to form product **C** (Figure 2). This is analogous to the migration of CH₃ from As to O that
363 we observed to be responsible for clean-up with TMA¹⁴. In this elementary step two As-O bonds are
364 broken, promoting formation of the O-H (1.0 Å) bond and the O-C bond (1.4 Å). Two electron-deficient
365 surface metal cations are forced to interact and as a result a metallic As-As dimer is formed along with
366 the intermediate ||As – NCH₃CH₂ – O||. Electrons are transferred to surface arsenic (+1.0e and +1.1e on
367 the dimer atoms) from the C atom of CH₂ (-1.6e) but also from N (-0.5e), elongating the N-As bond by
368 around 2% as compared to structure **A**. Decomposition of the alkylamide via this process is thus
369 reducing the As oxide surface and contributing to clean-up. This oxidation of the C atom is endothermic
370 for most of the precursors: tantalum, titanium, zirconium amides (+0.8, +0.6, +0.3 eV respectively),
371 almost neutral for hafnium amide (+0.1 eV) and exothermic for magnesium amide (-0.8 eV) according
372 to equations (2) + (3) ($\Delta E'_{\text{clean-up}}$, Table 2). It is less favorable than formation of the As-C bond in the
373 structure **B** described above.

374 For completeness we studied scission of the C-H bond and the transfer of H to an As site. This process
375 essentially involves hydride (H⁻) dissociation from the alkylamide ligand and formation of products **D**
376 and **E** with structures illustrated in Figure 2. In the intermediate **D** two new bonds are created: As-H and
377 As-C, increasing the coordination number of the As atom from three to five. Formation of these two
378 bonds is expected to cause the withdrawal of the electronic density from the oxide substrate and so its
379 local oxidation (see scheme in Figure 4). Charge analysis suggests a decrease in electronic populations
380 by only -1.0e on the oxidised pentacoordinated As and an increase of +1.0e on the H atom bonded to
381 this arsenic. The absence of charge transfer between this arsenic and CH₂ suggests some charge
382 retraction that is explained as follows. The CH₂ moiety of the created surface product ||As – N(Me)CH₂

383 – As|| becomes more Lewis acidic ($-0.4e$ on the C atom) and the N atom more Lewis basic ($+0.5e$),
 384 attracting each other (4% shorter N-CH₂ bond, relative to the same bond in **B**) and repelling bonded
 385 arsenic atoms (both: As-N and As-CH₂ bonds are elongated by 4%, relative to the same bonds in **B** or
 386 **C**). This indicates that desorption of the N-methylmethylenimido ligand as neutral Me-N=CH₂ should
 387 be preferred over formation of the dianion ($[-N(Me)CH_2-]^{2-}$ and substrate oxidation. The oxidation of
 388 As upon hydride dissociation is not favorable. In fact this is one of the least favorable processes that we
 389 have computed with energy ranging from +1.6 eV to +1.0 eV for almost all of the precursors and
 390 energetically neutral only for Mg[N(CH₃)₂]₂. We observe that no As-O bond is broken in this
 391 elementary process, *i.e.* it does not contribute to clean-up.

392 Our results indicate that energy for hydride dissociation can be lowered by 0.9 eV when this process is
 393 accompanied by oxidation of the C atom and formation of the surface product **E**: ||As – NCH₃CH₂ – O||
 394 + ||As – H. In this case As-H and O-C bonds are formed breaking one As-O bond (see Figure 2). We
 395 note that electronic densities are withdrawn from the O-CH₂-N entity ($-1.0e$) by the newly-formed
 396 hydride ($+1.0e$) and there is no charge transfer to the substrate. The attack of CH₂ onto the O site and
 397 transfer of H⁻ to the As site is slightly endothermic for most of the precursors (+0.7 to +0.1 eV) and
 398 exothermic for the magnesium precursor (-0.9 eV).

399 DFT calculations show that decomposition of alkylamide ligand through scission of the C-H bond α to
 400 N is thermodynamically feasible, but requires quite high activation energy. This pathway is often
 401 referred to in the literature as β -H elimination²⁷. Most likely this process will result in hydroxylation of
 402 the native oxides and formation of C-As(Ga, In) bonds (**B**). A possible volatile product of this clean-up
 403 transformation is N-methyl methyleneimine (MMI). Desorption of imine in the considered system
 404 requires reorganization in the electronic density with the formation of an N=C double bond and
 405 cleavage of As-N and As-C bonds, which is consistent with a high activation energy (+1.4 eV for the Hf
 406 case; see above). Simultaneously, charge transfer to the surface As should occur resulting in formation
 407 of metallic As-As bonds. We calculate that desorption of imine according to the reaction: ||As –

408 $\text{NCH}_3\text{CH}_2 - \text{As}|| \rightarrow ||\text{As-As}|| + \text{CH}_3\text{NCH}_2 (g)$ costs +0.7 eV relative to formation of **B**. Thus, the
409 computed reaction energies and high activation energy for the first step suggest that this clean-up
410 pathway producing imine needs elevated temperature for activation.

411 The weakening effect of the N-lone pair on the C-H bonds in the α position has been observed in
412 vibrational spectroscopy, where an unusually low frequency of vibration of the C-H mode in TDMAH
413 has been reported²⁸. The C-H dissociation is possible already upon adsorption of alkylamide precursors
414 onto silicon substrates at very low temperature of 220 K²⁹. As mentioned in the previous section MMI
415 is a detected product of etching GaAs surface by TDMAAs^{25a}. Several reports can be found where
416 metal alkylamides are shown to decompose to produce imine and amine³⁰. We show here that H
417 elimination can occur from a ligand that has migrated to the native oxide surface (**A** \rightarrow **B**). Product **B**
418 can then undergo other transformations **B** \rightarrow **H-K**, leading to different clean-up products as described
419 later, or desorption of imine can occur. Either process leads to arsenic oxide removal and/or reduction to
420 metallic arsenic, and so may contribute to the clean-up effect.

421 Another clean-up product that can arise from H elimination in the structures **D** and **E** is arsine, AsH_3 .
422 However, the unfavourable energetics computed by DFT for elementary steps leading to surface
423 functionalization with $||\text{As} - \text{H}$ groups suggests that formation of arsine from intermediate **D** or **E** is a
424 minor clean-up channel.

425 3.3.2. *N-C scission (F-G)*

426 We next examined possible pathways for CH_3 dissociation resulting with products **F** and **G** (for
427 pathways see Figure 4, for structures of products Figure 2). First we considered activation of the N-C
428 bond in the presence of the available Lewis basic O site of the substrate (**F**). As the CH_3 group
429 coordinated to the N atom in the alkylamide ligand has Lewis acidic character (formally CH_3^+ ,
430 methylium cation), we expect no redox during transfer to the substrate in this step. Upon this transfer
431 the As-O bond is broken, promoting formation of a double bond between the As and N atoms (1.7 Å).
432 Our results indicate that the reaction along this pathway is moderately endothermic with a

thermodynamic energy of +1.0 to +0.4 eV for Ta, Ti, Zr, Hf, Al precursors and exothermic by -0.6 eV for the Mg precursor ($\Delta E'_{\text{clean-up}}$, Table 2).

Another possibility is for the CH₃ moiety to attack an As surface site (**G**). The DFT calculations show that, similarly, an As=N double bond is formed, but As-O bonds are not affected. We observe oxidation of the As atom (-1.9e), which is now pentacoordinated, and reduction of the C atom of the dissociated CH₃ moiety (+1.9e), consistent with transfer as CH₃⁻ (methanide anion). This elementary step is therefore the reverse of clean-up. The bond formed between the C atom and the As atom is 1.9 Å long. This decomposition structure is a little more unstable than **F** with respect to reactants, at a calculated energy difference of +0.1 eV relative to the energy for formation of product **F**.

Pathways involving dissociation of the methyl group lead to functionalization of the surface with ||O – CH₃ (**F**) or formation of the ||As – CH₃ groups (**G**) along with the ||As = NCH₃ fragment. This can thus lead to desorption of gaseous dimethyl ether, O(CH₃)₂, or trimethylarsine, As(CH₃)₃. Additionally, if a source of protons is present, methane CH₄ can be formed from ||As – CH₃. However, our calculations show that elementary steps for **F** and **G** formation that could give dimethyl ether or trimethylarsine as clean-up products are less competitive when compared to the elementary steps leading to formation of TDMAAs or MMI (**A** or **B**, see Table 2). During ALD of metal oxide films, protons can derive from the H₂O pulse, but are supposedly eliminated in reaction with alkylamide ligands to produce amine, the main ALD product. ||O-H groups are also formed during the H elimination process investigated above. We will see later that the sequence of production of **B** and **G** *intermediates* is competitive and can directly lead to methane production.

3.4. Further decomposition of dma ligand

3.4.1. Multiple redox steps – dehydrogenation H-I

Based on the results shown above, we assume that the main reaction channel for the elimination of H atoms from alkylamide ligands on the oxide substrate is formation of the surface hydroxide and carbon-arsenic bound *intermediate* as in product **B**. In this section we investigate the most stable products of successive dehydrogenation of the alkylamide ligand.

459 The stability of the surface intermediate **H** decreases by about 0.7 eV relative to **B** after a second proton
 460 transfer. The electronic density increases on both C atoms (+1.2e and +1.3e) and a total of two protons
 461 are transferred to the oxide surface. There are now two CH₂ entities that form bonds with acidic As
 462 atoms through basic C atoms. A loss of electronic density on N of -0.5e is observed in Bader analysis.
 463 This affects the As-N bond, which is weakened (about 8% longer than the As-N bond in product **B**)
 464 suggesting that the π character of this bond decreases. The lone pair of electrons on N is no longer
 465 stabilized and N becomes nearly pyramidal in this structure (see Figure 2). This process requires energy
 466 and so it is clear that it requires some thermal activation.

467 Further dehydrogenation is possible via carbon disproportionation yielding a methyldiyne fragment
 468 (HC) that inserts into the C-N bond in the intermediate **I**. The surface product features a double bond
 469 between As and N (1.7 Å) that is now bound to a vinyl moiety CH=CH₂ (C=C bond length: 1.3 Å).
 470 Three hydroxide groups and an As-As dimer with the bond length of 2.5 Å are formed at the expense of
 471 four As-O bonds. Bader analysis confirms reduction of the dimer As atoms (+1.1e and +1.4e for the As
 472 atoms bound to N) which means that this reaction contributes to clean-up. We also observe
 473 disproportionation of charge between C atoms (increase of electronic population on methylene group of
 474 +0.6e and decrease on methyldiyne group of -0.3e relative to populations on methyl groups in amide
 475 ligand in structure **A**). We note some charge transfer to the N atom of +0.5e. Formation of an
 476 [=NCH=CH₂]²⁻ adsorbate is the most endothermic of the considered processes (+1.6 eV relative to **B**
 477 formation).

478 Our computations thus show that successive dehydrogenation becomes progressively less favored. It
 479 may result in the formation of the following volatile products: imine from species **B** as mentioned
 480 above; aziridine, HN(CH₂)₂, from **H**; ethylene, C₂H₄, and subsequently molecular nitrogen, N₂, from **I**.
 481 The energetics for pathways leading to desorption of these species suggest that this is only possible
 482 through thermal activation – moderate temperatures for imine formation and high temperatures for
 483 desorption of molecular nitrogen.

484 Aziridine may be produced from structure **H** by a reaction of cleaving As-C bonds, forming a C-C bond
 485 (for this process we calculate +0.5 eV relative to formation of **H**), subsequent coupling with adjacent
 486 protons if available and desorption, all of which has a DFT energy of just +0.3 eV relative to **H**. This
 487 contributes to clean-up, leaving the surface with metallic As-As bonds according to: $\parallel\text{As} - \text{N}(\text{CH}_2 -$
 488 $\text{As}\parallel)_2 + \parallel\text{O} - \text{H} \rightarrow \parallel\text{As} - \text{O}\parallel + \parallel\text{As} - \text{As}\parallel + \text{HN}(\text{CH}_2)_2 \text{ (g)}$. The rate limiting step may be breaking As-C
 489 and forming a three membered C-C-N ring. Aziridine is one of the stable products detected in the *in situ*
 490 mass spectroscopy experiment of thermal decomposition of TDMAAs below 450°C ^{30b}.

491 C₂H₄ was detected as a desorption product originating from secondary surface reactions when a
 492 tantalum surface was exposed to Ta[N(CH₃)₂]₅ at 550 K ²⁷. One of the proposed mechanisms envisages
 493 dehydrogenation of methyleneimido intermediates, insertion of a methyldiyne moiety into the carbon-
 494 nitrogen bond and subsequent hydrogenation of the vinyl fragment to produce ethylene and leave an
 495 adsorbed N atom ²⁷. We suggest that, on the reducible arsenic oxide substrate following coupling of
 496 adsorbed N atoms to form N₂ could be possible at highly elevated temperatures, which would result in
 497 clean-up according to: $2 \parallel\text{As} = \text{NCH}=\text{CH}_2 + 2 \parallel\text{O} - \text{H} \rightarrow \parallel\text{As} - \text{As}\parallel + 2 \text{C}_2\text{H}_4 \text{ (g)} + \text{N}_2 \text{ (g)}$.

498 **3.4.2. Multiple redox steps J-K**

499 In this section we study sequences of CH₃ dissociation and alkylamide dehydrogenation reactions that
 500 give rise to new clean-up products. Assuming, as previously, that the most probable pathway for
 501 alkylamide dehydrogenation is arsenic oxide hydroxylation, we can consider pathways where the CH₃
 502 group formally dissociates either as the methylium cation or as the methanide anion (as the above
 503 investigation of processes producing **F** and **G** revealed a competition between them). Here we show the
 504 most stable products of these reactions. All other possible reactions can be found in the supporting
 505 information.

506 Our investigations suggest that the more stable products are those formed during reactions that do not
 507 involve charge transfer to the oxide substrate. For instance, dehydrogenation of the alkylamide ligand
 508 followed by dissociation of the methanide anion in structure **J** (Figure 1) is preferred over dissociation
 509 of the methylium cation that combined with proton dissociation results in substrate reduction: [–

510 $\text{N}(\text{CH}_3)_2^- \rightarrow [-\text{N}=\text{CH}_2]^- + [\text{CH}_3]^+ + [\text{H}]^+ + 2e^-$ (not showed in Figure 1). The step leading to product **J** is
 511 among the few steps that we find to be exothermic or neutral at 0 K for most of the regarded precursors
 512 (Table 2). The reorganized electron density in the proton dissociation process (see section 3.3.1 for
 513 description of the proton elimination process in structure **B**) can be attracted by a CH_3 group instead of a
 514 CH_2 group. Bader analysis shows an increase in the electronic populations on the C atom of CH_3
 515 ($+1.9e$) and decrease on the C atom belonging to the methylene moiety ($-1.2e$). The acidic methylene
 516 forms a double bond with the N atom (1.3 \AA), instead of bonding to surface cation like in structure **B**.
 517 The basic methanide bonds with the As atom (2.0 \AA). We note some increase of electronic density on
 518 the N atom that is now even more basic ($+0.5e$) than in the original alkylamide ligand in structure **A**.
 519 Proton dissociation accompanied by the formation of the methanide anion could be a low temperature
 520 channel for the formation of CH_4 . According to our computations formation of methane from surface
 521 intermediate **J** is slightly exothermic with energy -0.1 eV (neglecting entropy). CH_4 was observed in
 522 some studies as a product of decomposition of the amido ligands. Infrared (IR) spectroscopy and
 523 temperature-programmed desorption (TPD) investigations of $\text{Ti}[\text{N}(\text{CH}_3)_2]_4$ on a Si substrate showed that
 524 methane desorbs at temperatures below 400 K ^{29b}. In the same study DFT calculations suggest that
 525 facile generation of methane right above room temperature is due to the surface activation of C – H and
 526 C – N bonds of amido ligand. In the thermal chemistry investigation of $\text{Ta}[\text{N}(\text{CH}_3)_2]_5$ CH_4 is a
 527 decomposition product detected throughout the studied temperature range up to 600 K ²⁷. Our DFT
 528 results suggest that scission of the N-C bond is triggered by the H elimination process on the oxide
 529 substrate and thermodynamically is not as demanding as other decomposition processes. Although
 530 formation of methane is plausible, desorption of this chemical alone from the oxidised III-V system
 531 does not directly result in self-cleaning. In this pathway methane is formed according to: $\parallel\text{As} - \text{Me} + \parallel\text{O}$
 532 $- \text{H} \rightarrow \parallel\text{As} - \text{O} \parallel + \text{CH}_4$, so arsenic oxygen bonds are formed. However, other products can arise as a
 533 consequence of saturation of the native oxide surface with $[-\text{N}=\text{CH}_2]^-$ groups after CH_4 desorption in
 534 species **J**: C_2H_4 and subsequently N_2 . Eventual desorption of CH_4 , C_2H_4 and N_2 would finally lead to
 535 clean-up resulting in reduction of arsenic oxide to metallic arsenic, but involving multiple redox steps: 2

536 $\parallel\text{As} - \text{N}=\text{CH}_2 \rightarrow \parallel\text{As} - \text{As}\parallel + \text{C}_2\text{H}_4_{(g)} + \text{N}_{2(g)}$. This process requires energy to break the double bond
537 between N and C atoms, combining two CH_2 groups and two N moieties on the surface. As remarked in
538 our discussion of possible products arising from *intermediate I*, processes involving multiple redox
539 steps are presumably possible at highly elevated temperatures.

540 Further dehydrogenation of the methylene group in the $[-\text{N}=\text{CH}_2]^-$ adsorbate described above, yields a
541 methylidyne (CH^+) ion in surface product **K**. This is less favored by +1.0 eV relative to previous
542 process **J** (see Table 2). Proton dissociation to another O site renews C basicity (+1.0e with respect to
543 the $[-\text{N}=\text{CH}_2]^-$ adsorbate) that now can attack another As site. The $[-\text{N}=\text{CH}-]^{2-}$ ion is bound to surface
544 arsenic atoms through N and C, forming bonds 1.9 Å and 2.0 Å long respectively (**K** Figure 1).
545 Generation of the $[-\text{N}=\text{CH}-]^{2-}$ surface intermediate can directly lead to desorption of hydrogen cyanide,
546 HCN, another clean-up product: $\parallel\text{As} - \text{N}=\text{CH} - \text{As}\parallel \rightarrow \parallel\text{As} - \text{As}\parallel + \text{HCN}_{(g)}$. HCN was detected to
547 desorb at 600 K during tantalum alkylamide exposure to a tantalum substrate²⁷.

548 3.5 Effect of substrate on clean-up

549 Our model supposes that clean-up can be achieved by successive dissociation of ligands from the
550 absorbed precursor. One can expect that the $M - L$ bond can be easily activated on the oxide surface
551 when the substrate metal oxide is less stable than the deposited metal oxide $M_2\text{O}_n$. The metal center of
552 the precursor then becomes chemically active towards penetrating the III-V oxide substrate and
553 scavenging the oxygen. A similar technique is used for equivalent-oxide-thickness scaling for
554 complementary metal–oxide–semiconductor devices³¹. With different variations scaling is achieved via
555 a scavenging reaction between the scavenging element (metal) and SiO_2 and the driving force is also
556 formation of the metal oxide rather than maintaining SiO_2 . We showed previously that the driving force
557 of the clean-up effect is removing $\text{As}(\text{Ga}, \text{In}) - \text{O}$ bonds and forming $M - \text{O}$ bonds^{14, 31}. As has lower
558 electropositivity and therefore lower affinity to O than the metals considered: Mg, Hf, Zr, Ti, Ta and Al.
559 In thermodynamic equilibrium, formation of any of the oxides of these metals is assumed to be favored
560 over formation of the As oxide. DFT energetics for the ligand exchange mechanism supports this
561 supposition, independent of the ligand in use (see Figure 3 **A**, **A'** and **A''**). Among the III-V elements

(As, Ga, In) it is again As that has the lowest electropositivity and forms the weakest oxides. To emphasize this we calculate from first principles bulk energies for ligand exchange between the regarded precursors and Ga(III) and In(III) native oxides and compare them with the exchange energy for As(III/V) native oxide:

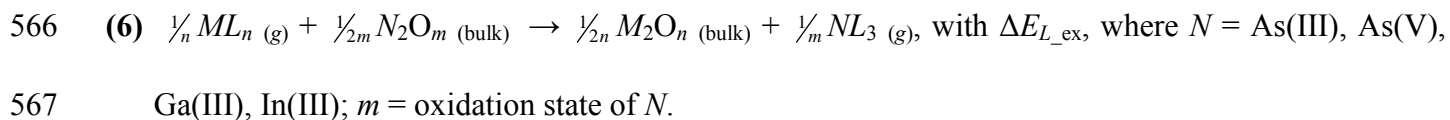
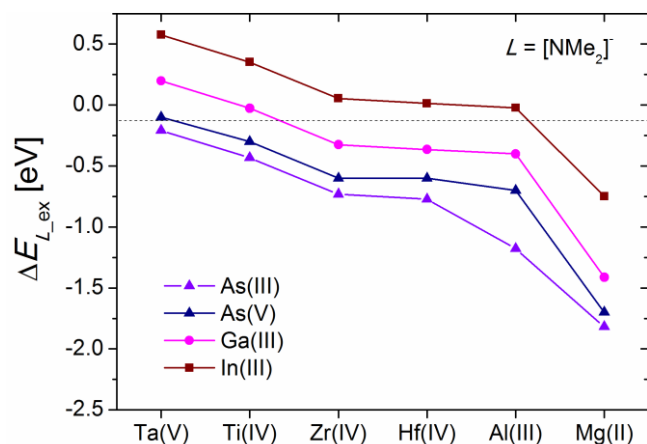
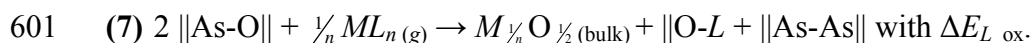


Figure 5 shows the energetics for the above reaction on the example of alkylamide precursors ($L = [\text{NMe}_2]$). It is clearly seen that As_2O_3 is the weakest and the most reactive among these native oxides towards exchanging O with ligands and therefore is the easiest to clean-up. It seems that In oxide resists clean-up more than Ga oxide and is less likely to bind to ligands at the surface. As(III) and As(V) oxides are seen to have similar reactivity for ligand exchange, with the exception of $\text{Al}[\text{NMe}_2]_3$ that seems to have greater affinity for As(III). We observe no oxidation state dependency for the ligand exchange mechanism, contrary to the suggestion of Hinkle *et al*⁸. This result holds true for different ligands (see supporting information).

Figure 5. Computed energetics for ligand exchange of alkylamide between precursor metal center and bulk III-V oxide: As_2O_3 , As_2O_5 , Ga_2O_3 and In_2O_3 according to: $\frac{1}{n}ML_n(g) + \frac{1}{2m}N_2O_m(\text{bulk}) \rightarrow \frac{1}{2n}M_2O_n(\text{bulk}) + \frac{1}{m}NL_3(g)$ for $M = \text{Mg(II)}$, Al(III) , Ti(IV) , Zr(IV) , Hf(IV) , Ta(V) , $L = [\text{N}(\text{Me})_2]^-$; n = oxidation state of M ; $N = \text{As(III)}$, As(V) , Ga(III) , In(III) ; m = oxidation state of N . Lines are to guide the eye.



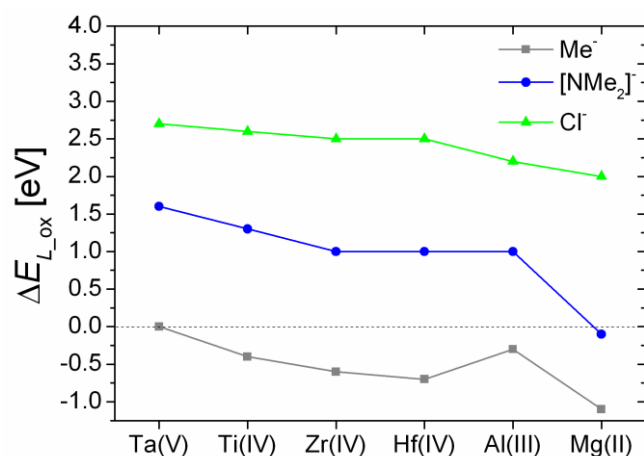
Additionally, ligands left on the surface can enhance the clean-up effect by interacting with the substrate and this depends on the affinity of the ligand to the substrate and on the chemical character of the substrate. We consider first ligand affinity. Metalloid oxides, like AsO_x , are susceptible to reduction in contact with reducing agents, *e.g.* by the methanide anion Me^- in TMA as we showed previously¹⁴ or by CH_2 from deprotonated alkylamide (section 3.3.1, C). Self-cleaning by TMA was shown to be governed by mobility of the methyl group, which undergoes oxidation, transferring electrons to the surface. Various elementary steps were found to be thermodynamically competitive and to lead to a surprising range of by-products. However, dma $[\text{NMe}_2]^-$ and chloride Cl^- anions are not as strong reducing agents as Me^- . This is supported by DFT energies, shown in Figure 6, for reactions of transferring those ligands from the metal center of the precursor to a surface O site on the As_2O_3 substrate. Formation of $\parallel\text{O}-L$ surface intermediates causes reduction of metalloid oxides:



602 In Figure 6 we can see that the chloride ligand, almost independently of which metal center it is bound
 603 to, is resistant to oxidation with ΔE_{L_ox} around +2.5 eV. The same holds for dma with $\Delta E_{L_ox} \approx +1.2$ eV,
 604 except for $Mg(NMe_2)_2$ that can dissociate its ligand to the O in the As_2O_3 substrate with ΔE_{L_ox} a little
 605 below 0 eV. On the contrary, the methyl group is always susceptible to oxidation with exothermic
 606 ΔE_{L_ox} for all metal precursors selected.

607

608 Figure 6. Computed energetics for ligand oxidation at the surface, $L = [N(Me)_2]^-$, $[Me]^-$, $[Cl]^-$, and
 609 As_2O_3 reduction according to: $||As-O|| + \frac{1}{n}ML_n(g) \rightarrow M\frac{1}{n}O\frac{1}{2}(bulk) + ||O-L + ||As-As||$ for $M = Mg(II)$,
 610 $Al(III)$, $Ti(IV)$, $Zr(IV)$, $Hf(IV)$, $Ta(V)$. Lines are to guide the eye.



611

612

613 The second factor affecting clean-up is substrate chemistry. If a ligand is susceptible to decomposition,
 614 specific sites on the surface can activate some bonds of the ligand and this can trigger secondary surface
 615 reactions that result in clean-up. C-H and N-C bonds of the dma ligand can be activated even at
 616 relatively low temperature as discussed in previous sections. It has been shown that especially mixed
 617 nucleophilic-electrophilic character of the surface sites, *e.g.* the zwitterionic character of silicon, affects
 618 reactivity and transformations of alkylamides²⁹. Such reactivity of alkylamides is confirmed by
 619 experimental observation of formation of Si-H bonds accompanied by the formation of Si-C bonds

(leading to incorporation of carbon into the deposited film). Low temperature production of methane has also been observed, which is evidence for N-C reactivity when depositing oxide films on bare Si or hydrogen terminated Si substrates. In our calculations, we see similar behaviour of the alkylamide ligand on the relatively weakly amphoteric As_2O_3 substrate. On this oxide substrate H is removed from the ligand as a proton and formation of O-H bonds is plausible. In this process clean-up is achieved, as well as producing additional reactive sites (OH) for ALD, but at the same time M-C bonds are formed. This is because proton elimination causes changes in electronic density on alkylamide carbons: the CH_2 fragment becomes Lewis basic and this promotes M-C formation (**B**), or the CH_3 fragment attracts the charge, and CH_3^- detachment is promoted, resulting also in M-C formation (**J**). Some of these reactions may be more strongly favoured on the mixture of more electropositive Ga^{3+} and In^{3+} sites of the real III-V surfaces or even the M^{n+} sites of the growing film, where bonds tend to be more ionic rather than covalent. Based on this we can conclude that the above-mentioned mechanisms account for the reactivity and behaviour of metal alkylamides and can be expected on various substrates featuring Lewis acid/base sites.

An important aspect is whether these processes occur during homodeposition (*i.e.* during the later stages of growth of *e.g.* HfO_2 onto HfO_2) and give a CVD component to standard ALD. Clearly during homodeposition there is no extra driving force from $M_2\text{O}_n$ formation. On the other hand, decomposition reactions may be more favoured on the growing film owing to its pronounced nucleophilic-electrophilic or Lewis acid/base character, as mentioned above. According to our computations, processes yielding **B-K** are energetically uphill from formation of intermediate **A** onwards. However the formation of **B** and **J** are only +0.5 eV and +0.8 eV uphill respectively at 0 K for the clean-up process on the As_2O_3 substrate and can be expected at elevated temperatures. This finding is supported by experimental observation of increased efficiency of clean-up with increased temperature. Another aspect is simple consideration of the strength of the As-O bond and, using the example of HfO_2 , the Hf-O bond. Clearly the Hf-O bond, once it is formed, is much stronger and less reactive, which does not favour subsequent

645 CVD reactions. An explicit investigation of CVD reactions on the HfO_2 surface is necessary to fairly
646 judge the importance of the CVD contribution in case of alkylamide ALD, but is beyond the scope of
647 this paper.

648 4. Conclusion

649 We successfully apply our model for clean-up to explain differences in the performance of various
650 classes of precursor chemicals in removing native oxide from III-V substrates. Building on the example
651 of TMA, we identify two separate factors governing the clean-up effect: formation of the metal oxide as
652 the primary driving force and affinity of the precursor ligand to the III-V oxide substrate as the ancillary
653 force. That allows an efficient description of interactions of the various precursor ligands with an
654 oxidised III-V substrate, and of the associated multi-step chemical processes that lead to formation of
655 the clean-up products. We map out reaction sequences for the alkylamide ligand that lead plausibly to
656 products that are detected experimentally (aziridine, ethylene, MMI, HCN, methane). Through this
657 approach, a set of general reactions is generated and comparison is made between several different
658 precursors, including metal alkylamides $\text{Mg}[\text{N}(\text{CH}_3)_2]_2$, $\text{Al}[\text{N}(\text{CH}_3)_2]_3$, $\text{Ti}[\text{N}(\text{CH}_3)_2]_4$, $\text{Zr}[\text{N}(\text{CH}_3)_2]_4$,
659 $\text{Hf}[\text{N}(\text{CH}_3)_2]_4$, $\text{Ta}[\text{N}(\text{CH}_3)_2]_5$; metal methyls: $\text{Mg}(\text{CH}_3)_2$, $\text{Al}(\text{CH}_3)_3$, $\text{Ti}(\text{CH}_3)_4$, $\text{Zr}(\text{CH}_3)_4$, $\text{Hf}(\text{CH}_3)_4$,
660 $\text{Ta}(\text{CH}_3)_5$; and metal chlorides: MgCl_2 , AlCl_3 , TiCl_4 , ZrCl_4 , HfCl_4 , TaCl_5 . We can therefore predict the
661 best reagent for achieving the clean-up effect.

662 We predict that the investigated methyl precursors are the best reagents for deposition of dielectrics and
663 performing clean-up. Unfortunately, most of them are very unstable compounds. Clean-up is most
664 effective when depositing MgO , as Mg^{2+} works as the most effective scavenger of O^{2-} . Clean-up with
665 metal chlorides seems to have a fundamentally different mechanism, probably involving removal of the
666 O from the native oxide film and passivation with Cl groups.

667 The first principles study shows that clean-up with metal alkylamides has a similar mechanism to clean-
668 up with metal methyls as regards the scavenging of oxygen from weak As, Ga and In oxides. Arising
669 from this, ligand exchange can in principle lead to a clean-up product: tris(dimethylamino)arsine.

670 However steric hindrance and the bulky character of the alkylamide ligand are rate limiting factors,
671 which in this case are very pronounced and suggest that this particular reaction will not proceed.

672 Our study also shows the difference in mechanism underlying the consumption of III-V oxides with
673 alkylamido precursors from the one taking place with TMA. In the case of the alkylamide ligand,
674 thermal decomposition rather than migration of the entire ligand on the oxide surface is dominant,
675 taking into account the bulky character of the ligand and its known reactivity in contact with a
676 semiconductor or metallic surface. Clean-up of the reducible As oxide substrate is therefore enhanced
677 by secondary decomposition surface reactions, not by oxidation of the entire alkylamide. The H
678 elimination process that forms hydroxyl groups and As-C bound species (**B**) is exothermic or neutral at
679 0 K and kinetically demanding. The migration of these decomposition intermediates from an As site to
680 an O site (**C**) and direct reduction of the substrate is only slightly endothermic. Successive
681 dehydrogenation though becomes progressively less favored. Instead, the first H elimination may be
682 followed by another plausible reaction – N-C bond scission (**J**), which can lead to low temperature
683 methane production, albeit without the clean-up effect. Thermal activation is needed for formation and
684 desorption of products that arise from these decomposition structures: most likely N-
685 methylmethyleimine and aziridine, possibly along with methane, ethylene and dinitrogen. A specific
686 requirement of the substrate is that it contain both Lewis acid and Lewis base sites, which can activate
687 secondary surface reactions of ligands that are susceptible to decomposition, like the dimethylamido
688 group. These redox processes do lead to the reduction of arsenic oxides to metallic arsenic, which in
689 turn can reduce gallium and indium oxides to pure III-V material. Some of the reactions that we have
690 presented therefore account for the clean-up effect, but they occur in parallel with reactions that do not
691 achieve clean-up.

692 More generally we show that organometallic reagents react readily with substrates featuring less
693 electropositive metals. In presence of metals like Si, As, Ga and In, a reactive polar metal-organic ligand
694 bond, *e.g.* Al-C, is broken and formation of more covalent bond, *e.g.* As-C, is favoured. These reactions

695 might be possible during homodeposition and can thereby give a CVD component to standard ALD, as
696 is well-documented for alkylamides. The mechanisms described here are in line with observations on Si
697 surfaces as well. The same mechanisms can therefore be expected on other substrates, such as oxides
698 and nitrides, that show a mix of Lewis acid/base sites.

699

700 ASSOCIATED CONTENT

701 **Supporting Information Available:** lattice parameters and space groups, along with *k*-point
702 sampling for optimised bulk structures; geometrical parameters for optimised gaseous molecules;
703 additional list of possible clean-up *intermediates* that are formed during ALD III-V substrate exposure
704 to alkylamide metal precursors – energetics for the interaction of dma ligand with the substrate (ΔE_L);
705 surface models showing products of the dissociative adsorption of Hf[N(CH₃)₂]₄ precursor; reaction
706 profile for dissociative adsorption of Hf[N(CH₃)₂]₄ precursor; energetics for ligand exchange between
707 precursor metal centre and bulk III-V oxide: As₂O₃, As₂O₅, Ga₂O₃ and In₂O₃ for *L* = [Me][−]; [Cl][−].

708 This material is available free of charge via the Internet at <http://pubs.acs.org>.

709

710 AUTHOR INFORMATION

711 Corresponding author

712 *E-mail address: simon.elliott@tyndall.ie.

713 Notes

714 The authors declare no competing financial interest.

715

716

717

718 ACKNOWLEDGMENT

719 This work was funded by Science Foundation Ireland under grant no. 07/SRC/I1172 (“FORME”,
720 www.tyndall.ie/forme). The authors wish to acknowledge the SFI/HEA Irish Centre for High-End
721 Computing (ICHEC) for the provision of computational facilities and support.

722

723 REFERENCES

- 724 1. Miikkulainen, V.; Leskela, M.; Ritala, M.; Puurunen, R. L., Crystallinity of inorganic films
725 grown by atomic layer deposition: Overview and general trends. *Journal of Applied Physics* **2013**, *113*
726 (2), 021301-101.
- 727 2. Huang, M. L.; Chang, Y. C.; Chang, C. H.; Lee, Y. J.; Chang, P.; Kwo, J.; Wu, T. B.; Hong, M.,
728 Surface passivation of III-V compound semiconductors using atomic-layer-deposition-grown Al₂O₃.
729 *Applied Physics Letters* **2005**, *87* (25), 252104-3.
- 730 3. (a) Chang, C. H.; Chiou, Y. K.; Chang, Y. C.; Lee, K. Y.; Lin, T. D.; Wu, T. B.; Hong, M.;
731 Kwo, J., Interfacial self-cleaning in atomic layer deposition of HfO₂ gate dielectric on In_{0.15}Ga_{0.85}As.
732 *Applied Physics Letters* **2006**, *89* (24), 242911-3; (b) Delabie, A.; Brunco, D. P.; Conard, T.; Favia, P.;
733 Bender, H.; Franquet, A.; Sioncke, S.; Vandervorst, W.; Van Elshocht, S.; Heyns, M.; Meuris, M.; Kim,
734 E.; McIntyre, P. C.; Saraswat, K. C.; LeBeau, J. M.; Cagnon, J.; Stemmer, S.; Tsai, W., Atomic Layer
735 Deposition of Hafnium Oxide on Ge and GaAs Substrates: Precursors and Surface Preparation. *Journal*
736 *of The Electrochemical Society* **2008**, *155* (12), H937-H944.
- 737 4. (a) Granados-Alpizar, B.; Muscat, A. J., Surface reactions of TiCl₄ and Al(CH₃)₃ on GaAs(100)
738 during the first half-cycle of atomic layer deposition. *Surface Science* **2011**, *605* (13-14), 1243-1248; (b)
739 Gougousi, T.; Lacis, J. W., Native oxide consumption during the atomic layer deposition of TiO₂ films
740 on GaAs (100) surfaces. *Thin Solid Films* **2010**, *518* (8), 2006-2009.

741 5. Gougousi, T.; Ye, L., Interface Between Atomic Layer Deposition Ta₂O₅ Films and GaAs(100)
742 Surfaces. *The Journal of Physical Chemistry C* **2012**, *116* (16), 8924-8931.

743 6. (a) Tallarida, M.; Adelmann, C.; Delabie, A.; Van Elshocht, S.; Caymax, M.; Schmeisser, D.,
744 Surface chemistry and Fermi level movement during the self-cleaning of GaAs by trimethyl-aluminum.
745 *Applied Physics Letters* **2011**, *99* (4), 042906; (b) Lin, L.; Robertson, J., Defect states at III-V
746 semiconductor oxide interfaces. *Appl. Phys. Lett.* **2011**, *98* (8), 082903.

747 7. (a) O'Mahony, A.; Monaghan, S.; Chiodo, R.; Povey, I.; Cherkaoui, K.; Nagle, R.; O'Connor, E.;
748 Long, R.; Djara, V.; O'Connell, D.; Crupi, F.; Pemble, M.; Hurley, P. K., Structural and Electrical
749 Analysis of Thin Interface Control Layers of MgO or Al₂O₃ Deposited by Atomic Layer Deposition and
750 Incorporated at the High-k/III-V Interface of MO₂/In_xGa_{1-x}As (M = Hf|Zr, x = 0|0.53) Gate Stacks. *ECS*
751 *Transactions* **2010**, *33* (2), 69-82; (b) O'Mahony, A.; Monaghan, S.; Provenzano, G.; Povey, I. M.;
752 Nolan, M. G.; O'Connor, E.; Cherkaoui, K.; Newcomb, S. B.; Crupi, F.; Hurley, P. K.; Pemble, M. E.,
753 Structural and electrical analysis of the atomic layer deposition of HfO₂/n-In_{0.53}Ga_{0.47}As capacitors with
754 and without an Al₂O₃ interface control layer. *Applied Physics Letters* **2010**, *97* (5), 052904-3; (c)
755 O'Connor, E.; Brennan, B.; Djara, V.; Cherkaoui, K.; Monaghan, S.; Newcomb, S. B.; Contreras, R.;
756 Milojevic, M.; Hughes, G.; Pemble, M. E.; Wallace, R. M.; Hurley, P. K., A systematic study of
757 (NH₄)₂S passivation (22%, 10%, 5%, or 1%) on the interface properties of the Al₂O₃/In_{0.53}Ga_{0.47}As/InP
758 system for n-type and p-type In_{0.53}Ga_{0.47}As epitaxial layers. *Journal of Applied Physics* **2011**, *109* (2),
759 024101-10; (d) Monaghan, S.; O'Mahony, A.; Cherkaoui, K.; O'Connor, E.; Povey, I. M.; Nolan, M. G.;
760 O'Connell, D.; Pemble, M. E.; Hurley, P. K.; Provenzano, G.; Crupi, F.; Newcomb, S. B. In *Electrical*
761 *analysis of three-stage passivated In_{0.53}Ga_{0.47}As capacitors with varying HfO₂ thicknesses and*
762 *incorporating an Al₂O₃ interface control layer*, AVS: 2011; pp 01A807-8.

763 8. Hinkle, C. L.; Sonnet, A. M.; Vogel, E. M.; McDonnell, S.; Hughes, G. J.; Milojevic, M.; Lee,
764 B.; Aguirre-Tostado, F. S.; Choi, K. J.; Kim, H. C.; Kim, J.; Wallace, R. M., GaAs interfacial self-
765 cleaning by atomic layer deposition. *Applied Physics Letters* **2008**, *92* (7), 071901-3.

- 766 9. Gougousi, T.; Hackley, J. C.; Demaree, J. D.; Lacin, J. W., Growth and Interface Evolution of
767 HfO₂ Films on GaAs(100) Surfaces. *Journal of The Electrochemical Society* **2010**, *157* (5), H551-H556.
- 768 10. Frank, M. M.; Wilk, G. D.; Starodub, D.; Gustafsson, T.; Garfunkel, E.; Chabal, Y. J.; Grazul, J.;
769 Muller, D. A., HfO₂ and Al₂O₃ gate dielectrics on GaAs grown by atomic layer deposition. *Applied*
770 *Physics Letters* **2005**, *86* (15), 152904-3.
- 771 11. Milojevic, M.; Aguirre-Tostado, F. S.; Hinkle, C. L.; Kim, H. C.; Vogel, E. M.; Kim, J.;
772 Wallace, R. M., Half-cycle atomic layer deposition reaction studies of Al₂O₃ on In_{0.2}Ga_{0.8}As (100)
773 surfaces. *Applied Physics Letters* **2008**, *93* (20), 202902-3.
- 774 12. Elliott, S. D., Atomic-scale simulation of ALD chemistry. *Semiconductor Science and*
775 *Technology* **2012**, *27* (7), 074008.
- 776 13. Hegde, G.; Klimeck, G.; Strachan, A., Role of surface orientation on atomic layer deposited
777 Al₂O₃/GaAs interface structure and Fermi level pinning: A density functional theory study. *Applied*
778 *Physics Letters* **2011**, *99* (9), 093508-3.
- 779 14. Klejna, S.; Elliott, S. D., First-Principles Modeling of the “Clean-Up” of Native Oxides during
780 Atomic Layer Deposition onto III–V Substrates. *The Journal of Physical Chemistry C* **2012**, *116* (1),
781 643-654.
- 782 15. Kresse, G.; Furthmüller, J., Efficient iterative schemes for ab initio total-energy calculations
783 using a plane-wave basis set. *Physical Review B* **1996**, *54* (16), 11169.
- 784 16. Perdew, J. P.; Chevary, J. A.; Vosko, S. H.; Jackson, K. A.; Pederson, M. R.; Singh, D. J.;
785 Fiolhais, C., Atoms, molecules, solids, and surfaces: Applications of the generalized gradient
786 approximation for exchange and correlation. *Physical Review B* **1992**, *46* (11), 6671.
- 787 17. (a) Vanderbilt, D., Soft self-consistent pseudopotentials in a generalized eigenvalue formalism.
788 *Physical Review B* **1990**, *41* (11), 7892; (b) Kresse, G.; Hafner, J., Norm-conserving and ultrasoft
789 pseudopotentials for first-row and transition elements. *Journal of Physics: Condensed Matter* **1994**, *6*
790 (40), 8245.

- 791 18. Wyckoff, R. W. G., Crystal Structures. *Crystal Structures* **Wiley Interscience, New York,**
792 **1963.**
- 793 19. Ballirano, P.; Maras, A. Z., Refinement of the crystal structure of arsenolite, As₂O₃. *Kristallogr.-*
794 *New Cryst. Struct.* **2002**, *217*, 177-178.
- 795 20. Henkelman, G.; Arnaldsson, A.; Jónsson, H., A fast and robust algorithm for Bader
796 decomposition of charge density. *Computational Materials Science* **2006**, *36* (3), 354-360.
- 797 21. Henkelman, G.; Uberuaga, B. P.; Jonsson, H., A climbing image nudged elastic band method for
798 finding saddle points and minimum energy paths. *The Journal of Chemical Physics* **2000**, *113* (22),
799 9901-9904.
- 800 22. (a) Murray, C.; Elliott, S. D., Density Functional Theory Predictions of the Composition of
801 Atomic Layer Deposition-Grown Ternary Oxides. *ACS Applied Materials & Interfaces* **2013**, *5* (9),
802 3704-3715; (b) Elliott, S. D., Improving ALD growth rate via ligand basicity: Quantum chemical
803 calculations on lanthanum precursors. *Surface and Coatings Technology* **2007**, *201* (22–23), 9076-9081.
- 804 23. Suri, R.; Lichtenwalner, D. J.; Misra, V., Interfacial self cleaning during atomic layer deposition
805 and annealing of HfO₂ films on native (100)-GaAs substrates. *Applied Physics Letters* **2010**, *96* (11),
806 112905-3.
- 807 24. Lamagna, L.; Wiemer, C.; Perego, M.; Spiga, S.; Rodríguez, J.; Santiago Coll, D.; Grillo, M. E.;
808 Klejna, S.; Elliott, S. D., Mechanisms for Substrate-Enhanced Growth during the Early Stages of
809 Atomic Layer Deposition of Alumina onto Silicon Nitride Surfaces. *Chemistry of Materials* **2012**, *24*
810 (6), 1080-1090.
- 811 25. (a) Marx, D.; Asahi, H.; Liu, X. F.; Higashiwaki, M.; Villaflor, A. B.; Miki, K.; Yamamoto, K.;
812 Gonda, S.; Shimomura, S.; Hiyamizu, S., Low temperature etching of GaAs substrates and improved
813 morphology of GaAs grown by metalorganic molecular beam epitaxy using trisdimethylaminoarsenic
814 and triethylgallium. *Journal of Crystal Growth* **1995**, *150*, Part 1 (0), 551-556; (b) Salim, S.; Ping Lu,
815 J.; Jensen, K. F.; Bohling, D. A., Surface reactions of dimethylaminoarsine during MOMBE of GaAs.
816 *Journal of Crystal Growth* **1992**, *124* (1–4), 16-22; (c) Shi, B.; Tu, C., A kinetic model for

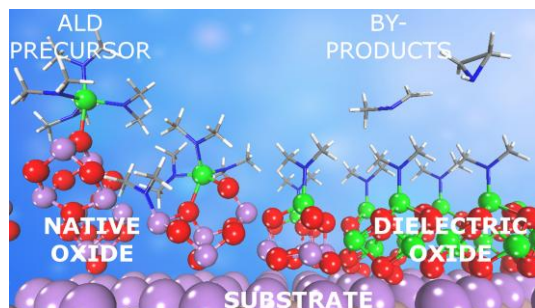
- 817 tris(dimethylamino) arsine decomposition on GaAs(100) surfaces. *Journal of Electronic Materials*
818 **1999**, 28 (1), 43-49.
- 819 26. Puurunen, R. L., Formation of Metal Oxide Particles in Atomic Layer Deposition During the
820 Chemisorption of Metal Chlorides: A Review. *Chemical Vapor Deposition* **2005**, 11 (2), 79-90.
- 821 27. Kim, T.; Zaera, F., Surface Chemistry of Pentakis(dimethylamido)tantalum on Ta Surfaces. *The*
822 *Journal of Physical Chemistry C* **2011**, 115 (16), 8240-8247.
- 823 28. Li, K.; Li, S.; Li, N.; Dixon, D. A.; Klein, T. M., Tetrakis(dimethylamido)hafnium Adsorption
824 and Reaction on Hydrogen Terminated Si(100) Surfaces. *The Journal of Physical Chemistry C* **2010**,
825 114 (33), 14061-14075.
- 826 29. (a) Rodríguez-Reyes, J. C., Mechanisms of adsorption and decomposition of metal alkylamide
827 precursors for ultrathin film growth. *J. Appl. Phys.* **2008**, 104 (8), 084907; (b) Rodríguez-Reyes, J. C.
828 F.; Teplyakov, A. V., Chemisorption of Tetrakis(dimethylamido)titanium on Si(100)-2 × 1: C-H and
829 C-N Bond Reactivity Leading to Low-Temperature Decomposition Pathways. *The Journal of Physical*
830 *Chemistry C* **2008**, 112 (26), 9695-9705.
- 831 30. (a) Bradley, D. C.; Chisholm, M. H., Transition-metal dialkylamides and disilylamides.
832 *Accounts of Chemical Research* **1976**, 9 (7), 273-280; (b) Salim, S.; Lim, C. K.; Jensen, K. F., Gas-
833 Phase Decomposition Reactions of Tris(dimethylamino)phosphine, -Arsine, and -Stibine Reagents.
834 *Chemistry of Materials* **1995**, 7 (3), 507-516.
- 835 31. Ando, T., Ultimate Scaling of High-κ Gate Dielectrics: Higher-κ or Interfacial Layer
836 Scavenging? *Materials* **2012**, 5 (3), 478-500.

837

838

839

840 TABLE OF CONTENTS (TOC)



841

842 Deleterious native oxides of semiconductor substrate are transformed into dielectric oxide when atomic

843 layer deposition technique (ALD) with the appropriate precursor chemical is used during transistor

844 fabrication.

845